AIP | Journal of Applied Physics

Accurate argon cluster-ion sputter yields: Measured yields and effect of the sputter threshold in practical depth-profiling by x-ray photoelectron spectroscopy and secondary ion mass spectrometry

Peter J. Cumpson, Jose F. Portoles, Anders J. Barlow, and Naoko Sano

Citation: J. Appl. Phys. **114**, 124313 (2013); doi: 10.1063/1.4823815
View online: http://dx.doi.org/10.1063/1.4823815
View Table of Contents: http://jap.aip.org/resource/1/JAPIAU/v114/i12
Published by the AIP Publishing LLC.

JOURNAL OF APPLIED PHYSICS **114**, 124313 (2013)

Accurate argon cluster-ion sputter yields: Measured yields and effect of the sputter threshold in practical depth-profiling by x-ray photoelectron spectroscopy and secondary ion mass spectrometry

Peter J. Cumpson, Jose F. Portoles, Anders J. Barlow, and Naoko Sano
National EPSRC XPS User's Service (NEXUS), School of Mechanical and Systems Engineering, Newcastle University, Newcastle upon Tyne, NE1 7RU, United Kingdom

(Received 30 July 2013; accepted 13 September 2013; published online 30 September 2013)

Argon Gas Cluster-Ion Beam sources are likely to become widely used on x-ray photoelectron spectroscopy and secondary ion mass spectrometry instruments in the next few years. At typical energies used for sputter depth profiling the average argon atom in the cluster has a kinetic energy comparable with the sputter threshold, meaning that for the first time in practical surface analysis a quantitative model of sputter yields near threshold is needed. We develop a simple equation based on a very simple model. Though greatly simplified it is likely to have realistic limiting behaviour and can be made useful for estimating sputter yields by fitting its three parameters to experimental data. We measure argon cluster-ion sputter yield using a quartz crystal microbalance close to the sputter threshold, for silicon dioxide, poly(methyl methacrylate), and polystyrene and (along with data for gold from the existing literature) perform least-squares fits of our new sputter yield equation to this data. The equation performs well, with smaller residuals than for earlier empirical models, but more importantly it is very easy to use in the design and quantification of sputter depth-profiling experiments. © *2013 AIP Publishing LLC*. [http://dx.doi.org/10.1063/1.4823815]

I. INTRODUCTION

Ion beam sputtering has been used for many years in conjunction with surface analytical techniques to provide profiles of composition as a function of depth. Surface layers are removed in a succession of sputtering steps, and x-ray photoelectron spectroscopy (XPS) or secondary ion mass spectrometry (SIMS) used to analyse the surface revealed. Until recently the ions of choice were monatomic, typically argon ions in XPS, though with a wider range of primary ion types being used in SIMS than in XPS. The energy range available using modern commercially available ion columns is typically in the range of 200 eV–5000 eV, with the lower energies being more widely used, especially in cases where surface damage that may change the chemistry of the sample must be minimised during analysis. Even the lowest of these energies is significantly above the threshold[1] for sputtering to take place, so that significant yields and therefore acceptable sputter rates are achieved.[2]

In the last few years gas cluster ion beam (GCIB) columns have begun to be commercially available, and, in particular, over the last year all of the main surface analysis instrument manufacturers have begun to make their own models of GCIB source available, at least on new instruments. Argon cluster ion sources were originally developed for semiconductor processing[3,4] and advanced coatings,[5] and subsequently the use of these sources for analytical applications was pioneered in SIMS.[6,7] They are likely to be at least as useful in XPS,[8] where for example sputter depth profiling of organic semiconductors[9] could, at least in principle, give access to defect and band bending measurements at interfaces. These GCIB sources produce ionised argon clusters having a size distribution ranging from around 500 to 5000 atoms. The average kinetic energy per atom (which we shall denote by ε_0) is much lower than for the monatomic ions used previously, leading to greatly reduced damage in sputter depth-profiling of polymers. The number of users of these GCIB sources is likely to increase rapidly, since the very low damage that these cluster ions introduce has been shown[10] to allow practical depth-profiling of polymer and other organic samples,[11] for the first time preserving almost all of the original sample chemistry. The very wide range of practical benefits this offers in many technological applications in polymer science, biomaterials, organic electronics, and photovoltaics amongst many others means that we are likely to witness a rapid increase in the number of users of these sources worldwide. In contrast to sputtering with monatomic ions, gas cluster sputtering may show threshold effects at energies commonly used in practical depth profiling. Cluster energies are often in the range $E = 2\,\text{keV}$–$20\,\text{keV}$, with clusters having a mean size range of $n = 500$ to 5000 atoms. The average energy per atom, $\varepsilon_0 = E/n$, in these clusters is comparable to typical covalent bond energies (of the order of 1 eV) so that one might expect a threshold (below which sputtering effectively ceases) in many aspects of routine depth-profiling for the first time. No analytical description currently exists, yet there is a pressing need to be able to estimate (or even predict accurately) sputter yields for cluster ions at these energies. The complexity of the interaction of gas clusters with a surface has meant that, until now, the approaches used to study this system have been either detailed molecular dynamics simulations[12] or modelling of experimental data using purely empirical relationships.[13–15] Clearly it is impractical to perform a careful molecular dynamics calculation in support of each depth-profiling experiment. A quantitative description of GCIB sputtering

near threshold would be extremely valuable, even if it were somewhat approximate. There is a body of published work on analytical estimation of monatomic sputter yields and thresholds[16–19] that can be of some guidance. Our aim is to develop an equation for estimating this total sputter yield based on a physical model. Such a model, even if greatly simplified, is likely to be more widely applicable (for example in limiting cases of high or low energy or new target material properties) than a purely empirical equation for sputter yield.

To validate our model we have made experimental measurements of sputter yield as a function of cluster energy for silicon dioxide, polystyrene (PS), and poly(methyl methacrylate) (PMMA) using quartz crystal microbalance (QCM) sensors. The model is greatly simplified and cannot compete with molecular dynamics modelling in terms of completeness; nevertheless, after fitting to experimental data we obtain parameter values that allow estimation of sputter yield for experimental planning and quantification of depth profiles for these materials.

II. SPUTTERING MODEL

Figure 1 shows schematically three steps in the impact of a single argon cluster ion. We will greatly simplify this process so as to obtain a simple equation for sputter yield, and then (replacing some of the parameters with "effective parameters" that may differ modestly from their true values) fit this equation to experimental data.

Consider the moment of impact illustrated in Fig. 1(b). The cluster loses coherence and may best be considered as n separate atoms having an average energy ε_0. This stage is still far from thermal equilibrium. If each atom were to have exactly this energy, then we would presumably observe a very sharp change in sputter yield for values of ε_0 close to threshold, as is the case for bombardment with monatomic ions. Instead there is certain to be a distribution of energies amongst the atoms released as the cluster disintegrates. It is probably not appropriate to model this as a thermal distribution as the system is far from equilibrium, but we may choose a Gaussian distribution of energy and see how well this matches experimental sputter-yield data. Therefore suppose the distribution of energy amongst the argon atoms in the small packet created at the moment of impact is $N(\varepsilon)$, where

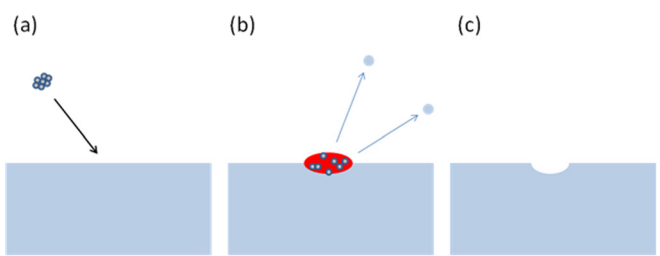

FIG. 1. Schematic diagram illustrating (a) approach of an argon cluster ion, (b) disintegration of the cluster around 0.5 to 5 ps after impact, and (c) the crater left by this single ion after a long period of time. Assuming a Gaussian distribution of argon atom energies at stage (b) allows us to derive a facile equation for sputter yield that can nevertheless be made useful by fitting its parameters to measured sputter yields.

$$N(\varepsilon)\mathrm{d}\varepsilon = \alpha \exp\left[\frac{-(\varepsilon-\varepsilon_0)^2}{s^2}\right]\mathrm{d}\varepsilon. \tag{1}$$

Here s is a measure of the spread of energies of individual argon atoms released at the disintegration of the cluster and α is a normalisation constant. We would expect a certain fraction of atoms having greater than the effective threshold energy U to be in a geometrically favourable position to remove one or more atoms from the surface by sputtering, and for that geometry not to change much as a function of energy. If this model were rigorously correct, and the collective motion of argon atoms and sputtered fragments could be ignored in favour of a sum of the effects of individual atomic sputtering events, then we could identify U with the atomic sputtering threshold energy E_{th}. We choose to use a different symbol, however, to emphasise that U is an effective parameter when using this one-atom sputtering model to fit experimental data. We know there is intense collective interaction at the site of sputtering, and this may mean the effective threshold differs from the monatomic threshold. We might expect $U \approx E_{th}$ in many cases, but U is very definitely an *effective* parameter. In this scheme we might expect the sputter yield to have the same approximately linear form as for monatomic sputtering, multiplied by the fraction of the atoms in the cluster that emerge from its disintegration with the effective sputter threshold energy, U, or greater, i.e.,

$$\frac{Y(\varepsilon_0)}{n} \propto \varepsilon_0 \int_U^\infty \exp\left[\frac{-(\varepsilon-\varepsilon_0)^2}{s^2}\right]\mathrm{d}\varepsilon, \tag{2}$$

so that

$$Y(\varepsilon_0) = n\varepsilon_0 A\left[1+\mathrm{erf}\left(\frac{\varepsilon_0-U}{s}\right)\right], \tag{3}$$

where A, U, and s are constants for a particular material. In this model of independent atomic sputtering by the atoms released by the disintegrating cluster ion, the total sputtering yield should be proportional to the number of atoms, n, in the cluster, for constant ε_0. This is consistent with earlier observations by Postawa *et al.*[20] amongst others that it is useful to plot $Y(\varepsilon_0)/n$ against ε_0/n. Such plots (as we shall see) show that clusters of different numbers of atoms give rise to data that follow roughly the same curve. Note that $n\varepsilon_0$ is simply the kinetic energy of the cluster, but since the energy occurs elsewhere in Eq. (3) as ε_0 it seems sensible to write it in terms of ε_0 alone.

Clearly the above model neglects all collective motion of fragments of the cluster and sputtered surface that we know takes place. Nevertheless, we might expect to be able to account for most of these effects by allowing the values of A, U, and s to deviate from their physically monotomic sputtering values to become effective parameters. Being so simple, the validity of using this model rests entirely on whether it fits experimental data to the accuracy required in practical depth-profiling using argon clusters and is useful in practical situations in which a rapid estimate of sputter yield to an acceptable accuracy is required.

III. CHOICE OF SPUTTER-YIELD MEASUREMENT METHOD

If we are to find values for the constants in Eq. (3) for a particular material then we need a good experimental method for measuring sputter-yield close to threshold, i.e., when that sputter-yield is very small. Ideally that method should be applicable to a wide range of different types of material and certainly to a wide range of polymers and oxides.

There are essentially three different methods used to measure total sputter yield:

(a) Depth-profiling through a uniform thin film of known thickness. This is generally easy to do and can be extremely precise, but requires a method of fabricating the thin film of the material under test and calibrating its thickness. Interferometry or atomic force microscopy (AFM) is often used for this thickness calibration, but the fabrication of a uniform film can nevertheless be a challenge for some materials. It can be prohibitively difficult to fabricate very thin layers of some materials.

(b) Produce a sputter-crater in a *bulk* sample of the material under test and measure the dimensions of the crater to estimate the volume of material removed for a known, measured beam current and sputter time. Depending on the method used to estimate the crater volume, this can often be more tolerant of a certain amount of surface roughness. However crater dimensions can be difficult to measure to the required accuracy if the crater volume is small, so long sputter times are often needed, and the method is not easy to apply close to the sputter threshold energy where the yield is small.

(c) Measure the mass lost from a bulk sample of the material during the formation of the sputter crater. This requires an extremely sensitive measurement of mass lost, in the nanogram range. Fortunately the quartz crystal microbalance is inexpensive and very suited to this. A coating of the material under test needs to be applied to the crystal surface before such work. Although it is a bulk sample (in the sense that one does not sputter completely through it) for the QCM to operate accurately, it needs to be in the range of a few tens of nanometres to a few micrometres in thickness, but need not be particularly uniform or low in surface roughness. The variation of sensitivity over the surface of the resonator can be a problem in quantification of measurements, and we pay particular attention to this issue in the work described below.

We have previously[21] measured GCIB sputter rates in polymers by method (b) combining contact masking and optical profilometry. However this would be difficult and inaccurate if applied to measuring the low sputter rates near threshold. Extremely long sputter times would be needed. Instead, in this current work, we have measured sputter rates *in situ* using a QCM—this has been used for many years to measure sputter rates from monatomic ion beams. It was first applied by McKeown,[22] barely a couple of years after the publication of Sauerbrey's original QCM work,[23] highlighting its sensitivity and therefore capability to measure sputtering yields near threshold. Careful studies of sputter threshold by this method have continued, with a relatively recent study by Wu *et al.*[24] using QCMs for this purpose. Navinšek *et al.*[25] used QCM for sputter measurements for a multilayer depth profile reference material.

IV. EXPERIMENTAL

To our knowledge the QCM method has not previously been used to measure cluster ion sputter rates, perhaps because, for inorganic materials at least, the sputter rates are so low that conventional oscillator QCMs do not offer sufficient precision or stability with respect to small changes in stray capacitance and temperature. Instead we have constructed a computer-based QCM instrumentation system based on a vector network analyser (Model Bode 100, Omicron, Klaus, Austria) and in-house software written in MATLAB for data recording and fitting. This allows us to fit each separate frequency scan around the fundamental resonant frequency of the QCM to a realistic equivalent circuit representation so that small changes in (for example) series resistance or parallel capacitance can be very effectively rejected. This system records an entire frequency sweep approximately every 50s. Multiple successive sweeps were performed, for periods between about 2 and 12 hours depending on the sputter rate of the material under test. Within these periods the coated crystal was exposed to known energy and beam currents of argon cluster ions, and the resulting steps in resonant frequency were subsequently extracted and quantified off-line by a separate MATLAB script. XPS spectra were recorded at intervals between sputtering steps to ensure the material composition was as expected.

The QCM measurements were performed *in situ* within our K-Alpha XPS instrument (Thermo Scientific, East Grinstead, UK) at our NEXUS facility, equipped with a Thermo MAGCIS argon cluster source. Our argon cluster source generates a range of cluster sizes. These pass through a Wien filter that selects clusters above a given size such that we can choose clusters of roughly $n = 1000$ or $n = 2000$ atoms per cluster. In XPS instruments we unfortunately do not have the ability to measure these cluster distributions directly (unlike most SIMS instruments), so to a large extent we must rely on calibration of the Wien filter conditions by the manufacturer to achieve these average cluster sizes.

QCM quartz crystals were placed in our own design of low-profile, low stress holder fabricated using only UHV compatible materials and no polymers or organic materials. This was mounted on the sample block supplied by Thermo Scientific designed for work-function measurements on semiconductors; while we conducted no such work function experiments, we used this block to give us electrical access to the QCM *in situ* during XPS and argon cluster-ion sputtering. Indeed, QCM measurements were made simultaneously with x-ray and gas cluster exposure without the introduction of significant additional noise. We used AT-cut quartz crystal sensors (Q-sense, Sweden) operated in the fundamental thickness-shear mode. These AT-cut crystal plates have a

relatively low temperature coefficient of resonant frequency at around room temperature. The arrangement of the QCM is shown schematically in Figure 2. Note that the large electrode of the QCM, on which the material under test lies, is always earthed. The material faces upwards and is sputtered from the cluster-ion gun at an angle of 58° to the surface normal. A 1 mm × 2 mm raster was used in sputter yield measurements, at a point at the centre of the large disc-shaped electrode on each QCM crystal. The centre point was determined carefully for each QCM crystal using the *in situ* optical microscope in the K-Alpha instrument.

Cluster-ion beam currents were measured using the electrometer built-in to the K-Alpha XPS instrument, but this was calibrated as follows. We used a Keithley 6221 current source which itself had recently been traceably calibrated to insert a set of dc currents of between −40 nA and +40 nA to the XPS instrument beam current electrometer. The response of the built-in electrometer was recorded. The output of the current source (although within calibration) was separately checked using a Keithley 6517A electrometer for complete confidence. All three instruments were in good agreement, though the K-Alpha electrometer showed a small nonlinear behaviour near zero current which we removed from subsequent measurements by means of a calibration curve.

The QCM crystals are commercially available with a number of different coatings for different sensor applications. The crystal plates we used are discs approximately 14 mm in diameter and thickness 300 μm, and have fundamental thickness-shear mode frequencies in the range 4.95 ± 0.05 MHz. Their surfaces are optically polished by the manufacturer, with a surface roughness of the electrode of less than 3 nm rms as measured by them. Such a low roughness may not be the case for the coated surface. These crystals have a large electrode on one side (with coating on top) and a smaller uncoated gold electrode on the other. The mass-per-unit-area and diameter of the smaller electrode determines the fundamental thickness-shear mode of vibration of the crystal plate, and hence the sensitive area of the crystal within the larger. This sensitive area is therefore always confined well inside the diameter of the larger, coated, electrode.

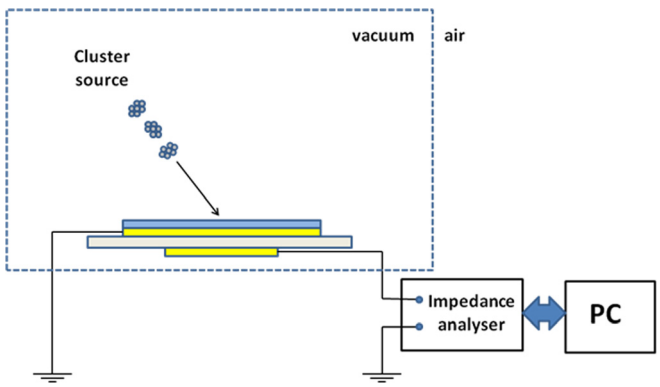

FIG. 2. Schematic experimental arrangement for sputter yield measurements. In between sputter steps we perform XPS analysis of the sputtered region to ensure that the gold electrode has not been reached (the x-ray source and analyser are not shown here). The angle of incidence is 58° to the surface normal. Gold electrodes are shown in yellow, and the sensitive area of the QCM effectively determined by the mass-per-unit-area of the smaller gold electrode on the underside of the crystal. The coating shown in blue on the top electrode is of the material whose sputtering properties are being studied.

In all of the measurements so far described we used the charge neutralisation system built-in to the K-Alpha XPS instrument. This is designed to stabilise surface potential so as to obtain good XPS spectra, and does so by exposing the surface to low energy electrons and low energy argon ions. Surface potentials—of either polarity—can be neutralised by attracting these ions and electrons. In normal XPS operation we find this neutralisation method to be very effective. We used the neutraliser in this work to (a) allow us to obtain good XPS spectra from insulating polymers between sputter steps and (b) ensure that the surfaces of these insulators are near earth potential to ensure the ion beam energy at the point that these ions impact the surface is the full accelerating voltage, not reduced by surface charging. A possible problem in using the neutraliser, however, is the damage such low energy ions and electrons may introduce. This damage could—at least in principle—change the sputter yield for argon clusters, for example by bond scission (which might be expected to increase the sputter yield) or by introducing crosslinks between polymer chains (which may be expected to reduce the sputter yield). To examine whether such an effect exists for our neutralisation conditions we performed two separate sputter treatments on two different PMMA-coated QCM crystals. The first underwent sputtering under eight different conditions (beam energy $E = 2$ kV, 4 kV, 6 kV, 10 kV, for average number of atoms per ion $n = 1000$ and 2000) with neutraliser and x-ray exposure throughout. The second PMMA crystal was at no point exposed to either neutraliser or x-rays, but only cluster-ion sputtering, under the same set of eight conditions. Both the x-ray source and flood gun were switched off during the cluster ion sputtering. PMMA was chosen because our previous work[26] has shown it to be particularly sensitive to x-ray enhanced cluster-ion sputtering,[27] probably due to the propensity of PMMA to degrade by "unzipping" or depolymerisation.[28] Therefore PMMA can be expected to be the most sensitive to damage—in the sense of processes likely to alter the sputter yield—than any other material we study in this work. Even so, the sputter yields we measured from both crystals agree to a standard deviation of 5%, except for the lowest sputter yield measurement (for $\varepsilon_0 = 1$ eV) where they differed by 13%, but which can readily be accounted for by the absolute uncertainties being larger for such a low yield. There was no systematic trend in the difference between the two sets of PMMA measurements that would suggest susceptibility to neutraliser.

V. TAKING ACCOUNT OF QCM SENSITIVITY VARIATION ACROSS ITS SURFACE

As we have shown previously,[29] to a very good approximation for AT-cut crystal sensors with sensitive area limited by the smaller of the two electrodes having diameter $2a$, the mass-sensitivity $c_f(r)$ at a radial distance r from the electrode centre is given by

$$c_f(r) = \begin{cases} c_0 J_0^2(k_1 r) & r \le a \\ c_0 [J_0^2(k_1 a)/K_0^2(k_2 a)] K_0^2(k_2 r) & r > a, \end{cases} \quad (4)$$

where $J_n(x)$ and $K_n(x)$ are the nth order Bessel functions, and c_0 is the mass sensitivity at the centre of the electrode, a constant for any given resonator

$$c_0 = \frac{f_0^2 K_0^2(k_2 a)}{\pi a^2 \rho_Q N_{AT} [K_0^2(k_2 a) J_1^2(k_1 a) + J_0^2(k_1 a) K_1^2(k_2 a)]}. \quad (5)$$

Here f_0 is the resonant frequency of the QCM sensor, N_{AT} is a constant for AT-cut plates, specifically, half the speed of transverse waves travelling normal to the plate, and ρ_Q is the density of quartz. Benes[30] gives the values $N_{AT} = 1661$ m/s and $\rho_Q = 2649$ kg/m^3. As explained in detail previously[31] k_1 and k_2 represent scalar approximations to the wavenumber for thickness-shear waves inside and outside the circular electrode, respectively. The wave number k_2 is given by

$$k_2 = \frac{\pi \sqrt{2 f_0 \Delta f_{elec}}}{N_{AT}}. \quad (6)$$

To confirm the applicability of Eqs. (4)–(6) we first mapped the sensitivity of the crystal surface experimentally. Figure 3 shows raw measured data from a PMMA coated QCM crystal. Each small step corresponds to a brief exposure to argon cluster ions of 6 eV/atom, followed by the QCM being moved one millimetre along a diameter of the crystal disc. The second set of steps is the result of repeating this process, but moving the crystal in the opposite direction. No ion beam raster was used.

Figure 4 shows these step heights plotted as a function of displacement across the diameter of the QCM. The continuous curve is calculated from Eqs. (4) and (6) and scaled in height to fit the experimental data (required since we do not have an independent measurement of the mass removed at each sputter step). Importantly this is the only adjustable parameter; agreement between measurements and theory over the shape of the sensitivity function c_f is excellent.

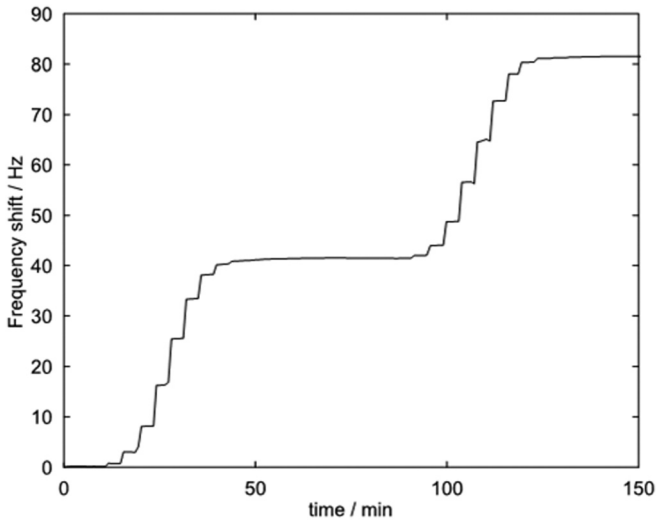

FIG. 3. Experimental measurements of QCM sensitivity as a function of position on its surface. Each small step in this frequency plot occurs when the surface is briefly sputtered. The stage holding the QCM is moved 1 mm along a diameter of the QCM crystal after each sputter step. Each sputter step represents the same fluence of ions so that the step height is proportional to QCM sensitivity at each point. The second series of steps, on the right, was recorded for these same points in reverse order, i.e., moving −1 mm each time.

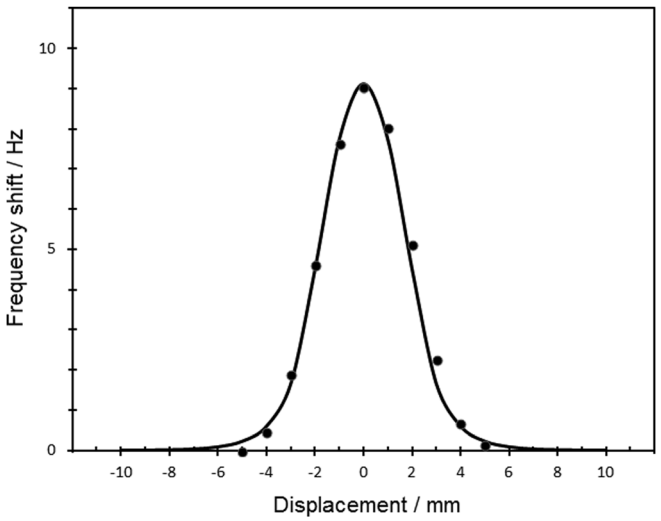

FIG. 4. Peak shifts shown in Fig. 3, plotted here as a function of displacement across the QCM surface. This shows the shape of the QCM response to small added masses as a function of position and allows us to calculate the mass of material removed from a given small raster area close to the centre of the QCM disc.

Having established the validity of this description of the variation of QCM sensitivity over its surface, we convolved the function described by Eq. (4) with a Gaussian of FWHM 0.65 mm, the FWHM we measured for the argon cluster ion beam spot using a Faraday cup. We then performed a numerical integration of the result of this convolution over the area of the cluster-ion beam raster (1 mm × 2 mm at the QCM centre) to determine the absolute sensitivity of the QCM in the ion exposed region. This then allowed us to calculate the absolute loss of mass for each set of ion beam conditions for similar QCM crystals having SiO_2, polystyrene, and PMMA layers.

VI. RESULTS AND DISCUSSION

Figures 5–8 show results for silicon dioxide, polystyrene, and PMMA coated crystals, and literature measurements for gold, including continuous lines representing least-squares fits to determine the three parameters in Eq. (3). Our QCM measurements are most appropriate for the lowest energy-per-atom range, and for practical reasons for some of the period during which these measurements were made our argon cluster-ion source could not be used above 6 keV per ion, so we also plot data taken from the literature extending to higher energies. This includes data from a recent paper by Rading *et al.*,[32] the recent Ph.D. thesis by Ichiki of Kyoto University,[33] from Yang *et al.*,[34] and from data plotted by Seah[13] from a forthcoming publication by Yang *et al*. In each case we have performed a least-squares fit in log-log space to Eq. (3), and in each case this fit seems very successful. Fitted parameter values are given in Table I.

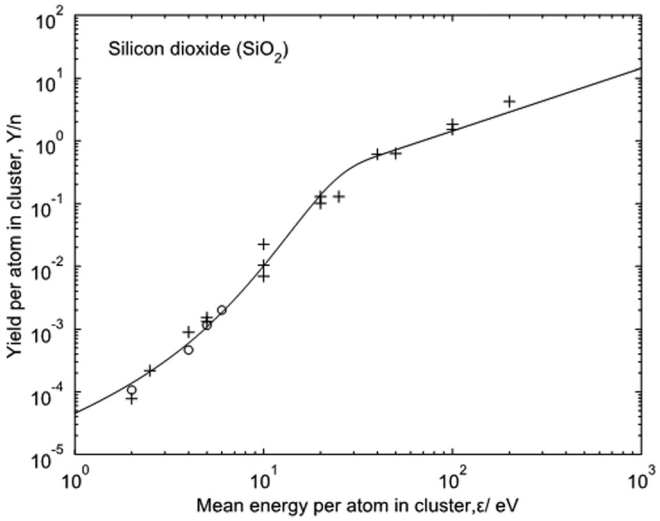

FIG. 5. Measurements of total argon cluster-ion sputter yield from silicon dioxide. Measurements shown are from this work (o) and from Seah[13] (+). The continuous line is a fit to Eq. (3).

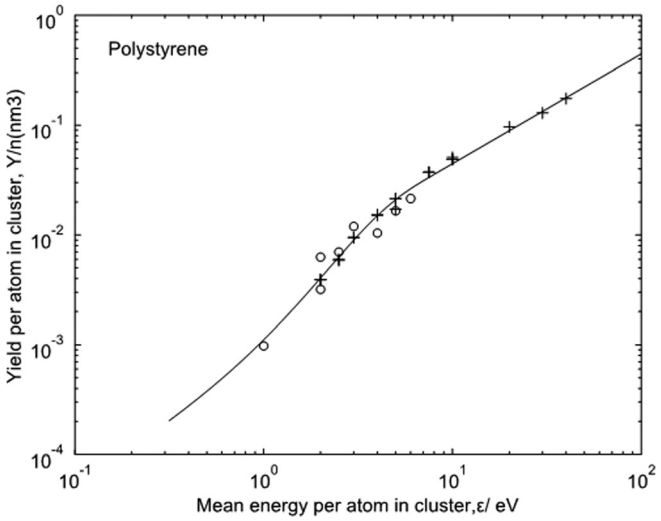

FIG. 6. Measurements of total argon cluster-ion sputter yield from polystyrene. Measurements shown are from this work (o) and from Rading *et al.*[26] (+). The continuous line is a fit to Eq. (3).

Figure 5 shows measurements for silicon dioxide. It is impressive that there is good agreement between measurements from two entirely different experimental methods used by different groups employing GCIB sources of different designs from two different manufacturers. Second, within the experimental uncertainties the approximation that $Y(\varepsilon_0) \propto n$ for a given ε_0 seems to hold well for this data. Third, a good fit to these measurements is achieved using Eq. (3).

Figure 6 shows measurements from our QCM method and from Rading *et al.*[26] These are in generally good agreement, though the QCM measurements show more experimental scatter. Nevertheless, the QCM data provides an extremely valuable measurement for the total sputter yield at $\varepsilon_0 = 1$ eV, which helps to improve confidence in the fitted parameters obtained when fitting to Eq. (3). Again, this fit appears valid.

Figure 7 shows data for poly (methyl methacrylate) from three sources. QCM again provides a valuable measurement at low energy. The measurements of Rading *et al.* have lower scatter. The data of Ichiki also show significant scatter, and it should be mentioned that Ichiki's measurements are for normally incident cluster-ions. Angular dependent studies (for example, Figure 3 of Rading *et al.* for polystyrene) suggest that there is little variation in total sputter yield between incidence angles of approximately 45°–60°, but this is not the case for lower emission angles and normal emission in particular. Nevertheless we have included Ichiki's data here as it is extremely valuable in providing information for much higher values of ε_0.

TABLE I. Fitted parameters for Eq. (3) for the four materials studied in this work.

	$A \times eV$	U/eV	s/eV
Silicon dioxide (SiO_2)	0.0072 atoms/ion	20.5	10.1
Gold	0.0032 atoms/ion	20.9	11.6
PS	0.0022 nm^3/ion	2.20	2.52
PMMA	0.0032 nm^3/ion	2.25	2.29

In Figure 8 we plot data from Yang *et al.*[28] alone. Since multiple measurements were made by Yang *et al.* for individual values of ε_0 (i.e., for different cluster sizes and energies) we have averaged the sputter yield to give a single plotted point for each value of ε_0. Also plotted in Fig. 8 are the results of two separate least-squares fits (in log-log space), first to Eq. (3) as in earlier cases, but here also to the recently proposed empirical equation by Seah.[13] Both models fit the data quite well, given the experimental scatter. The sum of the squared residuals overall are marginally lower for Eq. (3), but perhaps more significantly Eq. (3) performs better than the empirical fit below about $\varepsilon_0 = 20$ eV, which is the region of most importance in surface analytical applications. New designs of GCIB source for XPS and SIMS typically have maximum beam energies of 10 keV–20 keV and typical cluster sizes ranging from 1000 to 5000 atoms, so that for practical applications the region below $\varepsilon_0 = 20$ eV is the most important. Elsewhere[35] we have shown that the

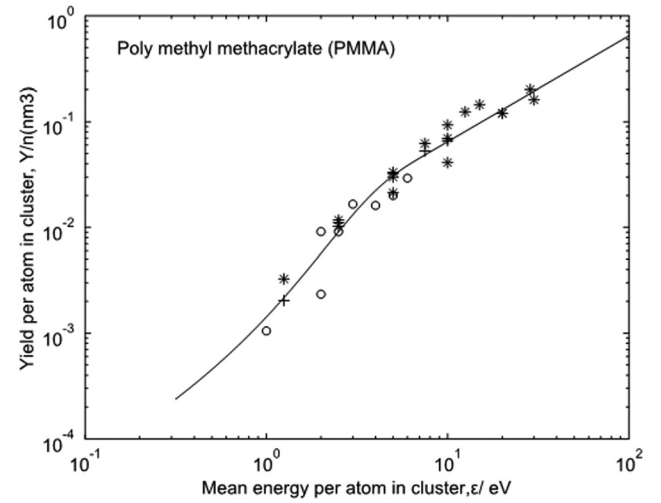

FIG. 7. Measurements of total argon cluster-ion sputter yield from PMMA. Measurements shown are from this work (o), from Rading *et al.*[26] (+) and from the thesis of Ichiki[27] (*). The continuous line is a fit to Eq. (3).

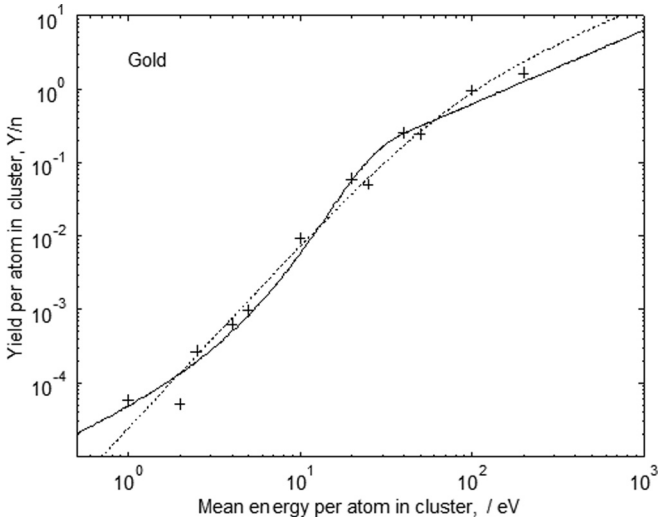

FIG. 8. Measurements of total argon cluster-ion sputter yield from gold. Measurements are from Yang *et al.*[34] (+). The continuous line is a least-squares fit to Eq. (3), and for comparison we also show (broken line) a least-squares fit to the empirical equation of Seah.[13]

region $3\,\text{eV} < \varepsilon_0 < 9\,\text{eV}$ is the most useful in terms of achieving good sputter rates simultaneously with good selectivity in the analysis of organic/inorganic interfaces.

We may now consider whether the parameter values obtained for PS, PMMA, gold and SiO_2 are reasonable in the context of other published data. For linear polymers such as PS and PMMA one might expect values for U of around (or perhaps slightly above) two times a typical covalent bond energy of around 1 eV, since at least two covalent bonds must be broken to release a sputtered fragment from a linear polymer. This is exactly what we have found, with values of 2.20 eV and 2.25 eV for PS and PMMA, respectively. For gold and SiO_2 the values of U are much higher, but very consistent with the monatomic ion sputter threshold data in the literature. For example, Wu *et al.*[24] find values of $E_{\text{th}} = 18\,\text{eV}$ and $E_{\text{th}} = 20\,\text{eV}$ for the sputter threshold of monatomic Ar^+ ions impacting a silicon target, from two theoretical models fitted to their measurements. For Ru and Mo targets they find a sputter threshold of $E_{th} = 33\,\text{eV}$ in both cases, though this is for normal incidence—one may expect a slightly lower value for the angles of incidence typical in XPS or SIMS. We conclude that—especially given the extreme simplicity of our model—the parameter values we obtain from experimental measurements are consistent with the latest monatomic sputtering measurements and suggest Eq. (3) may be very useful in predicting sputter yield at intermediate energies.

It is particularly striking that, for the four materials studied,

(i) The two inorganic materials (though very different) give very similar values for U and s.
(ii) For both inorganic materials $U \approx 2\,s$.
(iii) The two organic polymer materials (though very different) give very similar values for U and s.
(iv) For both organic polymer materials $U \approx s$.

We are currently in the process of making QCM measurements on a much wider range of materials to see which, if any, of these observations hold more widely.

VII. CONCLUSIONS

We have developed a quartz crystal microbalance system with a sensitivity and selectivity high enough to measure the argon gas cluster-ion sputter yields of inorganic and organic materials close to the sputter threshold for the first time. We propose a simplified model of sputtering at these energies, leading to Eq. (3), for estimating sputter yield in terms of three material-dependent parameters. We have fitted this equation to experimental data for four materials (silicon dioxide, gold, polystyrene, (PS), and PMMA). This model performs extremely well in these cases, suggesting that (with more data from more materials) it may become very useful for estimating total sputter yield for any given cluster size or energy of importance in surface analysis. This will be a major step forward in assisting experimental planning and retrospective quantification of cluster-ion sputter depth-profiles.

ACKNOWLEDGMENTS

Dr. J. F. Portoles is grateful for the support of the Newcastle/Durham EPSRC Knowledge Transfer Account (KTA). The authors would like to thank Mr. R. Burnett of the Mechanical Engineering School at Newcastle University for important advice and assistance with electrical measurements, and Dr. A. Horsfall of the Electrical Engineering School at Newcastle University for the loan of some of the electrical measurement equipment. XPS and GCIB sputtering were performed at the National EPSRC XPS User's Service (NEXUS) at Newcastle University, an EPSRC Mid-Range Facility.

[1]R. V. Stuart and G. K. Wehner, "Sputtering yields at very low bombarding ion energies," J. Appl. Phys. **33**, 2345 (1962).
[2]J. Bohdansky, "A universal relation for the sputtering yield of monatomic solids at normal ion incidence," Nucl. Instrum. Methods Phys. Res. B **2**, 587–591 (1984).
[3]I. Yamada, J. Matsuo, N. Toyoda, and A. Kirkpatrick, "Materials processing by gas cluster ion beams," Mater. Sci. Eng.: Rep. **34**, 231–295 (2001).
[4]L. P. Allen, T. G. Tetreault, C. Santeufemio, X. Li, W. D. Goodhue, D. Bliss, M. Tabat, K. S. Jones, G. Dallas, and D. Bakken, "Gas-cluster ion-beam smoothing of chemo-mechanical-polish processed GaSb(100) substrates," J. Electron. Mater. **32**, 842–848 (2003).
[5]A. J. Perry, S. J. Bull, A. Dommann, D. Rafaja, B. P. Wood, and M. Michler, "The surface damage in titanium nitride associated with lateral sputtering by argon cluster ions," Surf. Coat. Technol. **133–134**, 253–258 (2000).
[6]N. Winograd, Z. Postawa, J. Cheng, C. Szakai, J. Kozole, and B. J. Garrison, "Improvements in SIMS continue: Is the end in sight?," Appl. Surf. Sci. **252**, 6836–6843 (2006).
[7]C. M. Mahoney, "Cluster secondary ion mass spectrometry of polymers and related materials," Mass Spectrom. Rev. **29**, 247–293 (2010).
[8]T. Miyayama, N. Sanada, S. R. Bryan, J. S. Hammond, and M. Suzuki, "Removal of Ar^+ beam-induced damaged layers from polyimide surfaces with argon gas cluster ion beams," Surf. Interface Anal. **42**, 1453–1457 (2010).
[9]D.-J. Yun, C. Jung, H.-I. Lee, K.-H. Kim, Y. K. Kyoung, A. Benayad, and J. Chung, "Damage-free photoemission study of conducting carbon composite electrode using Ar gas cluster ion beam sputtering process," J. Electrochem. Soc. **159**, H626–H632 (2012).
[10]D.-J. Yun, J. Chung, C. Jung, K. H. Kim, W. Baek, H. Han, B. Anass, G. S. Park, S. H. Park, "An electronic structure reinterpretation of the organic semiconductor/electrode interface based on argon gas cluster ion beam sputtering investigations," J. Appl. Phys. **114**, 013703 (2013).
[11]N. Winograd, "Molecular depth profiling," Surf. Interface Anal. **45**, 3–8 (2013).

[12]A. Delcorte, B. J. Garrison, and K. Hamraoui, "Dynamics of molecular impacts on soft materials: From fullerenes to organic nanodrops," Anal. Chem. **81**, 6676–6686 (2009).
[13]C. Anders, H. M. Urbassek, and R. E. Johnson, "Linearity and additivity in cluster-induced sputtering: A molecular dynamics study of Van der Waals bonded systems," Phys. Rev. B **70**, 155404 (2004).
[14]T. Seki, T. Murase, and J. Matsuo, "Cluster size dependence of sputtering yield by cluster ion beam irradiation," Nucl. Instrum. Methods Phys. Res. B **242**, 179–181 (2006).
[15]M. P. Seah, "Universal equation for argon gas cluster sputtering yields," J. Phys. Chem. C **117**, 12622–12632 (2013).
[16]M. W. Thompson II, "The energy spectrum of ejected atoms during the high energy sputtering of gold," Philos. Mag. **18**, 377–414 (2010).
[17]Y. Yamamura and J. Bohdansky, "Few collisions approach for threshold sputtering," Vacuum **35**, 561–571 (1985).
[18]W. Eckstein, J. Roth, W. Nagel, and R. Dohmen, "Sputtering mechanisms near the threshold energy," J. Nucl. Mater. **328**, 55–61 (2004).
[19]Y. Yamamura and H. Tawara, "Energy dependence of ion-induced sputtering yields from monatomic solids at normal incidence," At. Data Nucl. Data Tables **62**, 149–253 (1996).
[20]Z. Postawa, R. Paruch, L. Rzeznik, and B. J. Garrison, "Dynamics of large Ar cluster bombardment of organic solids," Surf. Interface Anal. **45**, 35–38 (2013).
[21]P. J. Cumpson, J. F. Portoles, and N. Sano, "Material dependence of argon cluster ion sputter yield in polymers: Method and measurements of relative sputter yields for 19 polymers," J. Vac. Sci. Technol. A **31**, 020605-1 (2013).
[22]D. McKeown, "New method for measuring sputtering in the region near threshold," Rev. Sci. Instrum. **32**, 133–136 (1961).
[23]G. Sauerbrey, "Verwendung von Schwingquarzen zur Wägung dünner Schichten und zur Mikrowägung," Z. Phys. **155**, 206–222 (1959).
[24]S.-M. Wu, R. van de Kruijs, E. Zoethout, and F. Bijkerk, "Sputtering yields of Ru, Mo, and Si under low energy Ar^+ bombardment," J. Appl. Phys. **106**, 054902 (2009).
[25]B. Navinšek, P. Panjan, A. Žabkar, and J. Fine, "A comparison of sputtered Ni/Cr interface depth resolution as obtained by the quartz crystal microbalance mass loss method and Auger spectroscopy," J. Vac. Sci. Technol. A **3**, 671 (1985).
[26]P. J. Cumpson, J. F. Portoles, N. Sano, and A. J. Barlow, "X-ray enhanced sputter rates in argon cluster ion sputter-depth profiling of polymers," J. Vac. Sci. Technol. B **31**, 021208-1 (2013).
[27]P. J. Cumpson, J. F. Portoles, and N. Sano, "Observations on X-ray enhanced sputter rates in argon cluster ion sputter depth profiling of polymers," Surf. Interface Anal. **45**, 601–604 (2013).
[28]M. E. Fragalà, G. Compagnini, L. Torrisi, and O. Puglisi, "Ion beam assisted unzipping of PMMA," Nucl. Instrum. Methods Phys. Res. B **141**, 169–173 (1998).
[29]P. J. Cumpson and M. P. Seah, "The quartz crystal microbalance; radial/polar dependence of mass sensitivity both on and off the electrodes," Meas. Sci. Technol. **1**, 544 (1990).
[30]E. Benes, "Improved quartz crystal microbalance technique," J. Appl. Phys. **56**, 608–627 (1984).
[31]P. J. Cumpson, "Quartz crystal microbalance: A new design eliminates sensitivity outside the electrodes, often wrongly attributed to the electric fringing field," J. Vac. Sci. Technol. A **15**, 2407–2412 (1997).
[32]D. Rading, R. Moellers, H.-G. Cramer, and E. Niehuis, "Dual beam depth profiling of polymer materials: Comparison of C60 and Ar cluster ion beams for sputtering," Surf. Interface Anal. **45**, 171–174 (2013).
[33]K. Ichiki, "Study on size effect of cluster ion beam irradiation," Ph.D. thesis (Kyoto University, 2012).
[34]L. Yang, M. P. Seah, and I. S. Gilmore, "Sputtering yields for gold using argon gas cluster ion beams," J. Phys. Chem. **116**, 23735–23741 (2012).
[35]P. J. Cumpson, J. F. Portoles, A. J. Barlow, N. Sano, and M. Birch, "Depth-profiling organic/inorganic interfaces by argon gas cluster ion beams: Sputter yield data for biomaterials, in-vitro diagnostic and implant applications," Surf. Interface Anal. (to be published).